



Dexmedetomidine induces immunogenic cancer cell death and sensitizes tumors to PD-1 blockade

Liwei Zhao,^{1,2} Peng Liu,^{1,2} Allan Sauvat,^{1,2} Killian Carnet Le Provost,^{1,2} Jiani Liu,^{1,2} Andrea Checcoli,^{1,2} Jonathan Pol ,^{1,2} Oliver Kepp ,^{1,2} Guido Kroemer ,^{1,2} Lucillia Bezu ^{1,2}

To cite: Zhao L, Liu P, Sauvat A, *et al.* Dexmedetomidine induces immunogenic cancer cell death and sensitizes tumors to PD-1 blockade. *Journal for ImmunoTherapy of Cancer* 2025;**13**:e010714. doi:10.1136/jitc-2024-010714

► Additional supplemental material is published online only. To view, please visit the journal online (<https://doi.org/10.1136/jitc-2024-010714>).

Accepted 14 May 2025



© Author(s) (or their employer(s)) 2025. Re-use permitted under CC BY-NC. No commercial re-use. See rights and permissions. Published by BMJ Group.

¹INSERM UMR1138, Centre de Recherche des Cordeliers, Paris, France

²Metabolomics and Cell Biology Platforms, Gustave Roussy, Villejuif, France

Correspondence to
Dr Lucillia Bezu;
lucillia.bezu@gmail.com

Dr Guido Kroemer;
kroemer@orange.fr

ABSTRACT

Background Local anesthetics promote anticancer immune responses. A machine learning-based algorithm trained with information on the biological effects and molecular descriptors of analgesics, anesthetics, hypnotics and opioids predicted antitumor effects for dexmedetomidine (DEX). DEX is a sedative acting as an alpha2-adrenoceptor (ADRA2) agonist. Based on these premises, we investigated the putative antineoplastic effects of DEX.

Results In vitro, DEX promoted premortem stresses such as autophagy and partial endoplasmic reticulum stress with the phosphorylation of eukaryotic initiation factor 2 alpha and the inhibition of the splicing of X-box binding protein 1. DEX elicited the biomarkers of immunogenic cell death, including the release of ATP and high-mobility group box 1 protein, and the cell surface exposure of calreticulin, enhancing the engulfment of malignant cells by dendritic cells. In immunocompetent mice, DEX decreased the progression of colorectal cancers, fibrosarcomas, mammary carcinomas and melanomas, as it improved overall survival. These effects were inhibited by the ADRA2 antagonist yohimbine, suggesting that DEX mediates its anticancer effects at least in part on-target. Depending on the specific tumor model, DEX also enhanced the cytotoxic T cell/regulatory T cell ratio in the tumor bed and draining lymph nodes. Programmed cell death protein 1 blockade tended to improve DEX effects. After rechallenge with antigenically identical cells, no tumor appeared, indicating the formation of immunological memory.

Conclusions These results confirm the machine learning-predicted anticancer activity of DEX. Beyond its utility as a sedative agent in oncological intensive care, DEX may improve anticancer immunosurveillance and sensitize tumors to immune checkpoint blockade.

INTRODUCTION

Preclinical studies revealed that anesthetic agents can mediate anticancer effects by reducing the survival, proliferation and migration of malignant cells.^{1 2} Thus, local anesthetics and intravenous hypnotics such as propofol showed promising antineoplastic activities. These agents minimize tumor cell dissemination by inhibiting the production of angiogenic vascular endothelial growth

WHAT IS ALREADY KNOWN ON THIS TOPIC

⇒ Previous preclinical and clinical studies reported conflicting effects of dexmedetomidine (DEX), an alpha2-adrenoceptor (ADRA2) agonist, on cancer. Recent data indicate that various types of cancer cells express high ADRA2 levels and that ADRA2 agonists may induce antitumor effects.

WHAT THIS STUDY ADDS

⇒ An artificial intelligence-powered algorithm predicted that DEX-induced antitumor effects. This prediction was experimentally validated by showing that DEX killed cancer cells in vitro and induced anticancer responses in mice. These antineoplastic properties are mediated by ADRA2 and are often enhanced by combination with immune checkpoint blockers.

HOW THIS STUDY MIGHT AFFECT RESEARCH, PRACTICE OR POLICY

⇒ In oncology, periods requiring intensive care are conducive to tumor progression. Sedation with DEX might slow tumor growth during intensive care and hence prepare the grounds for curative cancer therapies after discharge.

factor (VEGF) as well as that of pro-metastatic matrix metalloproteinases (MMP-2, MMP-9) and E-cadherin.^{3 4} Both local anesthetics and propofol can stimulate intrinsic and extrinsic apoptotic pathways, interfere with cyclin-dependent kinases, or affect the epigenome of cancer cells.^{5–9} They also promote direct cytolytic effects on tumor cells by triggering different modalities of cell death such as apoptosis, ferroptosis and necrosis.^{10 11} Local anesthetics and propofol also suppress various oncogenic signaling pathways such as signaling transducer and activator of transcription 3/HOX antisense intergenic RNA, mitogen-activated protein kinase kinase, extracellular signal-regulated kinases/mitogen-activated protein kinases, and phosphoinositide 3-kinase/protein kinase B/mammalian target of rapamycin (PI3K/Akt/

mTOR).^{12–17} Moreover, local anesthetics and propofol directly act on immune effectors by favoring the proliferation of lymphocytes, maintaining the Th1/Th2 ratio, decreasing the action of immunosuppressive FoxP3⁺CD4⁺ T regulatory cells (Tregs) and myeloid-derived suppressor cells, and diminishing the synthesis of protumor cytokines such as IL-6.^{18–19} Moreover, local anesthetics can control inflammatory pain and immunosuppressive glucocorticoid stress.²⁰ After intratumoral injection of local anesthetics, dying cancer cells release danger-associated molecular patterns (DAMPs) that recruit and stimulate dendritic cells (DCs) to engulf and present tumor antigens to T cells. Activated cytolytic T lymphocytes then kill residual circulating malignant cells and promote an immune memory that avoids recurrences. The combination with anti-programmed cell death protein 1 (PD-1) antibodies potentiates this immune response, curing a fraction of mice bearing solid tumors.²¹

Conversely, morphine and hypnotic volatiles, tend to favor tumor progression by inhibiting phagocytosis, chemokine production, and cytolytic activity of natural killer cells, increasing the action of matrix metalloproteinases facilitating the migration, activating the *c-Myc* oncogene, promoting hypoxia-inducible factor (HIF-1 α) and VEGF expression, or enhancing PI3K/Akt/mTOR signaling pathway.^{22–25}

Dexmedetomidine (DEX), ((S)-4-[1-(2,3-dimethylphenyl)-ethyl]-1H-imidazole), is an α_2 -adrenoceptor (ADRA2) agonist with sedative properties that is widely used in veterinary and human medicine for intensive care and surgical procedures.^{26–28} DEX sedates without respiratory distress due to its action on ADRA2 located in the central nervous system without any stimulation of gamma-aminobutyric acid receptors.²⁹ Thus, DEX can be safely administered to mechanically ventilated patients, as well as to non-intubated patients. In addition, DEX reduces inflammation, controls nociception and promotes opioid-sparing effects. DEX represents an ideal alternative to common narcotics such as propofol and midazolam, and to morphine derivatives. In addition, DEX recently garnered interest due to the discovery of adrenoceptors on different types of cancer cells suggesting potential direct therapeutic effects.^{30–31} However, little is known about the potential procarcinogenic or anticarcinogenic effects of DEX in vivo.³²

A novel algorithm designed through a machine-learning approach that we describe here predicted DEX to mediate antineoplastic activity. As a result, we studied the putative anticancer effects of DEX. Our work unraveled that DEX has the capacity to kill cancer cells in an immunogenic fashion and to sensitize tumors to subsequent immunotherapy in preclinical models.

MATERIALS AND METHODS

Cell lines

Human osteosarcoma U2OS, human colon adenocarcinoma CT26, human lung cancer TC-1, human cervical

cancer HeLa, murine colon adenocarcinoma MC38, murine melanoma B16F10, murine breast cancer 4T1, murine RET melanoma cells, murine breast cancer E0771, and murine embryonic fibroblasts were supplied by American Type Culture Collection. Murine fibrosarcoma MCA205 cells were supplied by Merck. U2OS cells stably expressing green fluorescent protein (GFP)-light chain 3 (LC3), pSMALB-ATF4.5rep or XBP1 Δ DBD-Venus-red fluorescent protein (RFP)-FYVE and MCA205 cells expressing CD39 were previously generated in our lab.^{33–36} U2OS activating transcription factor 6 (ATF6)-GFP cell line was kindly given by Professor Peter Walter from the University of California, San Francisco, USA. Mycoplasma tests were regularly performed in all cell lines to control the absence of infection.

Cell culture

All cell lines were cultured in Dulbecco's Modified Eagle's Medium (#41 966–02, Thermo Fisher Scientific), except for the MCA205 cell line cultured in Roswell Park Memorial Institute 1640 medium (#61870044, Thermo Fisher Scientific). Media were supplemented with 10% fetal bovine serum (#F7524, Sigma-Aldrich), 1% non-essential amino acids (#11 140–035, Thermo Fisher Scientific), 1% HEPES (#15630080, Thermo Fisher Scientific), and 1% penicillin/streptomycin (#15140122, Thermo Fisher Scientific). For U2OS GFP-LC3, XBP1 Δ DBD-Venus-RFP-FYVE and ATF6-GFP cell lines, medium was supplemented with 0.5 mg/mL G418 (#10 131–27, Thermo Fisher Scientific) to maintain selection pressure. All cell lines were cultured in an incubator offering a stable humidified environment with 5% CO₂ and 37°C. The consumables required for the cell culture were purchased from Corning (New York, USA).

Compounds

Oxaliplatin was supplied by Accord Healthcare (Ahmedabad, India). DEX (PHR-2701), mitoxantrone (MTX) (M6545), necrostatin-1 (N9037), staurosporine (S6942), thapsigargin (T9033), and yohimbine (YOH) (Y3125) were supplied by Merck-Sigma Aldrich. Bafilomycin A1 (1334), torin 1 (4247) were supplied by Tocris Bioscience (Bristol, UK), and z-VAD-fmk (N1510.0025) was supplied by Bachem. LIVE/DEAD Fixable Yellow Dead Cell Stain Kit, for 405 nm excitation (#L34959) and eBioscience FoxP3/Transcription Factor Staining Buffer Set (#00-5523-00) were obtained from Thermo Fisher Scientific.

Antibodies

Rabbit polyclonal anti-calreticulin antibody (ab2907), rabbit monoclonal anti-phospho-eukaryotic initiation factor 2 α (eIF2 α) (Ser 51) antibody (ab32157, clone E90), mouse monoclonal anti-beta actin antibody (ab49900, clone AC-15) were obtained from Abcam (Cambridge, UK). Anti-mouse PD-1 antibody (BE0273, clone 29F.1A12), rat IgG1 isotype control, anti-horseradish peroxidase (BE0088, clone HRPN), rat IgG2b isotype control, anti-keyhole limpet hemocyanin

(BE0090, clone LTF-2), anti-CD4⁺ (BE0003-1, clone GK1.5) and anti-CD8⁺ (BE0061, clone 2.43) antibodies were obtained from BioXcell (West Lebanon, New Hampshire, USA). Anti-rabbit AlexaFluor 488 or AlexaFluor 647 coupled secondary antibody, rabbit polyclonal anti-ADRA2A (#PA5-120835), anti-ADRA2B (#PA5-109364), anti-ADRA2C (#PA5-114828) antibodies, rabbit monoclonal anti-CD31 antibody (#MA5-37858), mouse monoclonal anti-VEGF antibody (#MA5-13182) came from Thermo Fisher Scientific. BD OptiBuild RB780 hamster anti-mouse CD11c (#755338) was purchased from BD Biosciences; APC anti-mouse CD11c antibody (#117310), PE-Dazzle 594 anti-mouse LAG-3 antibody (#125224), AlexaFluor 700 anti-mouse CD45 antibody (#103128), APC-Fire750 anti-mouse CD8a antibody (#100766), BV650 anti-mouse CD25 antibody (#102038), and BV786 anti-mouse PD-1 antibody (#135225) were purchased from BioLegend; FITC anti-mouse FoxP3 antibody (#11-5773-82), PerCP-Cy5.5 anti-mouse CD3 antibody (#145-2C11), APC anti-mouse TIM-3 antibody (#17-5871-82), and eFluor450 anti-mouse CD4 antibody (#48-0042-82) were obtained from Thermo Fisher Scientific.

Western blot

The Western blot protocol was previously described in a study by Bezu *et al.*²¹

QSAR model establishment and exploration

A collection of 37 anesthetic agents was annotated according to their ability to induce antitumor (0) or protumor effects (1). Thereafter 1,875 molecular descriptors were computed using PaDEL software.³⁷ Variables with p value < 0.05 were retained (Mann-Whitney U test between the two groups exhibiting protumor and antitumor effects), leading to a data set of 37 labeled molecules associated with 605 descriptors. This data set was used for training a random forest (RF) binary classifier, using the *R caret* package, from which a confusion matrix was computed to evaluate model accuracy. In the next step, descriptors were weighted according to a decrease in the Gini index and used to generate a matrix based on Gower's similarity index by means of the *R daisy* package. Finally, this matrix was used to perform hierarchical clustering.

Viability assay

At day 0, U2OS, HT29, MCA205 and CT26 cells were cultured with 1,500 cells per well in a 384-well plate (Greiner Bio-one; Kremsmünster, Austria). At day 1, cells were treated with DEX for 8, 12 or 24 hours. Hoechst 33342, 1 µg/mL (H3570, Thermo Fisher Scientific) and propidium iodide, 1 µg/mL (P4864, Sigma-Aldrich) were used to stain the nuclei and assess viability, respectively. Cells were observed by live-cell microscopy (one acquisition/hour) using transmitted light, 4 6-diamidino-2-phenylindole (DAPI) staining, and Texas Red imaging filter sets. Analyses were performed with the R software (<https://www.r-project.org>) using the *EBImage*

package. The number of live cells was normalized for each condition to the number of live cells at T0.

Cell death assessment

At day 0, 8,000 U2OS wild-type cells per well were cultured in a 96-well plate. At day 1, cells were treated with DEX or staurosporine for 24 hours. Then, supernatants and cells were retrieved to assess cell death modalities following a described protocol.²¹

Fluorescence microscopy

At day 0, U2OS cells wild-type or U2OS cells stably expressing the following fusion proteins: GFP-LC3, pSMALB-ATF4.5rep, ATF6-GFP, XBP1ΔDBD-Venus-RFP-FYVE, were cultured with 1,500 cells per well in a 384-well plate. At day 1, cells were treated with DEX (25, 50, 100, 200, 400, 800 µM), thapsigargin (10 µM), torin (300 nM) and bafilomycin (100 nM). After treatment, cells were washed, fixed in paraformaldehyde (3.7% PFA, F8775, Merck-Sigma Aldrich) and stained with 1 µg/mL Hoechst 33342 (H3570, Thermo Fisher Scientific) for 20 min. U2OS wild-type cells were also stained with the anti-phospho-eIF2α antibody according to the protocol published in.²¹ Images were then acquired by fluorescence microscopy with a 20X Plan APO objective (Nikon, Tokyo, Japan) with appropriate filter sets in four fields of view (FOV) per well and processed with either the Custom Module Editor from MetaXpress Software (Molecular Devices) or custom R scripts using the EBImage package (<https://bioconductor.org/>). Briefly, nuclei regions were defined by thresholding the fluorescence signal from nuclear dyes, thereafter labeled using the watershed algorithm. When required, cytoplasmic regions were segmented using the same thresholding method with the adequate dye, and labeled using Voronoi's propagation method from labeled nuclei. Subcellular structures (such as "dots") were segmented by applying a top hat filter on the corresponding fluorescent micrograph, followed by thresholding. The obtained masks were thereafter used to compute nuclear (Hoechst 33342, ATF4, ATF6, XBP1s) and cytosolic features (eIF2α, ATF6, LC3) such as intensity, count and surface. The obtained single-cell data were processed using R software, after removing dead cells and debris based on nuclei area and Hoechst 33342 intensity.

Calreticulin translocation

At day 0, 1×10^6 U2OS wild-type cells per well were cultured in 6-well plates. At day 1, cells were incubated with the designed treatment for 8 hours. After treatment, the medium was changed to fresh medium and the cells were kept in culture for a further 16 hours. Then, cells were collected to assess calreticulin (CALR) translocation at the plasma membrane according to the protocol described in.²¹

HMGB1 release

At day 0, 1×10^6 mouse fibrosarcoma MCA205 wild-type cells per well were cultured in 6-well plates. At day 1, cells were treated for 24 hours with MTX (4 µM) or

DEX (600 μ M). Then, supernatants were retrieved and centrifuged. The concentration of high-mobility group box 1 (HMGB1) in the supernatants was assessed by ELISA (ST51011; IBL International GmbH, Hamburg, Germany). The results were calculated based on acquired absorbance (450 nm) with a SpectraMax i3 Multi-Mode Plate Reader (Molecular Devices).

Extracellular ATP assessment

8,000 U2OS wild-type cells per well were cultured in a 96-well plate. The day after, cells were treated with the appropriate treatments for 24 hours. Then, ATP release was assessed by means of a published luciferase luminescence protocol.²¹

Intracellular ATP assessment

At day 0, 8,000 cells per well were cultured in a 96-well plate. At day 1, cells were treated with the appropriate treatments for 24 hours. After treatment, cells were stained with 5 μ M quinacrine and 4 μ M Hoechst 33342 prepared in a Krebs-Ringer solution (125 mM sodium chloride, 5 mM potassium chloride, 0.7 mM monopotassium phosphate, 1 mM magnesium sulfate, 6 mM glucose, 2 mM calcium chloride, and 25 mM HEPES, pH 7.4) for 30 min at 37°C. Then, cells were washed with the Krebs-Ringer solution. Images were acquired with fluorescence microscopy using a 20X Plan APO objective (Nikon, Tokyo, Japan) in four FOV per well and processed with the MetaXpress software (Molecular Devices).

Phagocytosis assay

Bone marrow-derived dendritic cells (BMDCs) were obtained from the bone marrow extracted from the femurs of C57Bl/6J mice and prepared according to our protocol published in a study by Bezu *et al.*²¹ Mouse fibrosarcoma MCA205 wild-type cells were cultured with 8×10^5 cells in a 25 cm² flask and let adapt overnight in the incubator. Then, MCA205 cells were stained with 1 μ M CellTracker Orange CMTMR dye (#C2927, Thermo Fisher Scientific) for 30 min at 37°C and treated for 24 hours as designed. The next day, tumor cells and BMDCs were co-cultured in a 6-well plate at a 1:4 ratio (BMDC: MCA205) and kept in the incubator for 4 hours. Then, the co-cultured cells were collected and labeled with APC-conjugated antibody against CD11c (1:100 diluted in 1% bovine serum albumin, BSA) to identify DCs. Cells were kept in the dark for 30 min at 4°C. After three washes, cells were fixed in paraformaldehyde (3.7% PFA). A BD LSRFortessa flow cytometer linked to BD FACSDiva software (BD Biosciences) was used to analyze the data. Phagocytosis was defined by assessing CMTMR positive in CD11c positive cells (FlowJo software).

In vivo experiments

Immunocompetent female C57Bl/6J mice aged 6–8 weeks were obtained from Envigo (Huntington, UK). Mice were housed in a dedicated animal facility providing a temperature-controlled and germ-free environment. Food and water were given freely. The ‘BiostatTGV’

software was used to determine the optimal number of animals in each group. For each experiment, mice were randomized according to tumor size before treatment to avoid bias. The mathematical formula “width x length x $\pi/4$ ” was applied to calculate tumor size. Mice were sacrificed by cervical dislocation if tumor size was between 200 mm² and 250 mm², necrosis, weight loss >10% or signs of discomfort. The TumGrowth software package (<https://github.com/kroemerlab>) was used to compare tumor growth and survival curves.³⁸

In vivo treatment

Fibrosarcomas, breast tumors, colon adenocarcinomas and melanomas were generated after subcutaneous inoculation of 1×10^5 murine MCA205 cells, 1×10^6 murine E0771 cells, 1×10^6 murine MC38 cells, and 5×10^5 murine RET cells into immunocompetent female C57Bl/6J mice, respectively. As soon as tumors became detectable, mice were randomized according to the tumor sizes in each experiment. Then, the animals were treated with 25 μ l of DEX (diluted in phosphate-buffered saline (PBS)) or with PBS (negative control) injected intraperitoneally (*i.p.*) daily for 21 days or intratumorally (*i.t.*) every 3 days for 21 days. The tumor size and the weight of the mice were routinely monitored. At days 6, 9 and 12 after the first injection of DEX, 200 μ g/mouse of anti-PD-1 or the corresponding isotype (prepared in 50 μ l PBS) were injected *i.p.* At days –1, 0 and 7 before and after the first injection of DEX, 100 μ g/mouse of anti-CD4⁺ and anti-CD8⁺ or corresponding isotype (prepared in PBS) were injected *i.p.*

In vivo rechallenge

Mice bearing fibrosarcomas cured after the injections of DEX, alone or combined with immunotherapy (anti-PD-1), were rechallenged with the same cell type (1×10^5 murine fibrosarcoma MCA205 wild-type cells inoculated subcutaneously (*s.c.*) into one flank) and heterologous cells (1×10^6 murine colon adenocarcinoma MC38 wild-type cells inoculated *s.c.* into the contralateral site). One mouse bearing a colon adenocarcinoma that was cured by treatment with DEX+anti-PD-1, was rechallenged with the same cell type (1×10^6 murine colon adenocarcinoma MC38 wild-type cells) inoculated *s.c.* into one flank and heterologous cells (1×10^5 murine fibrosarcoma MCA205 wild-type cells) inoculated *s.c.* into the contralateral site. The tumor growth and the weight of the mice were routinely monitored.

Assessment of tumor and peritumor lymph node-infiltrating lymphocytes

Mouse MCA205 fibrosarcomas or mouse MC38 colon adenocarcinomas were induced after subcutaneous inoculation of 1×10^5 or 1×10^6 cells, respectively, into C57Bl/6J mice. As soon as tumors became detectable, PBS (25 μ l) or DEX (500 μ g/kg) was injected *i.p.* At day 9 post-injection, tumors were harvested, processed and stained according to our published protocol²¹ to assess tumor and peritumor lymph node infiltrating lymphocytes.

Assessment of tumor angiogenesis markers

MCA205 fibrosarcomas were induced after subcutaneous inoculation of 1×10^5 cells into C57Bl/6J mice. PBS (25 μ l) or DEX (500 μ g/kg) was injected *i.p.* when tumors became detectable. At day 9 post injection, tumors were harvested, fixed in paraformaldehyde (3.7% PFA, F8775 Sigma-Aldrich) and incubated in a solution of sucrose. Next, an ultramicrotome was used to cut 5 μ m sections of tumors. Tumor slices were then washed and blocked with glycine (100 mM) for 5 min followed by NH_4Cl (50 mM) for 20 min. VEGF and CD31 were assessed by immunostaining (rabbit monoclonal antibody anti-CD31 (#MA5-37858), mouse monoclonal antibody anti-VEGF (#MA5-13182) from Thermo Fisher Scientific). Representative images were acquired and data were analyzed using the QuPath V.0.5.1 software.

Statistical analyses

In vitro experiments: data shown represents mean of triplicates. When an experiment is presented as representative of three individual experiments, the results are presented as mean \pm SD. When three individual experiments are combined, the results are presented as mean \pm SEM. The statistics were produced using the R software (<https://www.r-project.org>). For parametric data, a student's *t*-test was applied to compare the conditions to a control (*t.test* function). When one condition was compared with another in a dataset, a pairwise test for multiple comparisons was used with a Benjamini-Hochberg correction (*pairwise.t.test* function).

In vivo experiments: the statistics were produced using the TumGrowth software package (<https://github.com/kroemerlab>).³⁸ Tumor growth was assessed with a type II analysis of variance test or a pairwise Wilcoxon test in case of multiple comparisons with a Holm correction. Survival analyses were determined with a log-rank test. For the tumor and peritumor lymph node immune infiltrates, statistical analyses were performed with the R software using a Wilcoxon-Mann-Whitney test or a pairwise Wilcoxon test in case of multiple comparisons with a Holm correction.

RESULTS

Identification of DEX as a bona fide antitumor agent

Previous studies demonstrated that local anesthetics can mediate direct or immune-dependent anticancer effects and hence improve overall and recurrence-free survival after oncological surgery.^{21,39} Other standard anesthetics, such as volatiles, opioids, or intravenous hypnotics had inconstant effects. Interestingly, unconventional antineoplastic molecules, such as metformin or beta-blockers, exert antitumor effects through off-target effects.⁴⁰ Driven by such target-agnostic considerations, we designed an algorithm using a machine learning approach to predict potential antitumor or protumor features of anesthetic agents. We first attributed a score to 37 anesthetics that had been characterized for their ability to predominantly

induce antitumor or protumor effects. Using the PubChem library (<https://pubchem.ncbi.nlm.nih.gov>), we then retrieved the structures of all clinically used anesthetics allowing us to compute their molecular descriptors using PaDEL software.³⁷ 605 descriptors were significantly ($p < 0.05$) different between the two categories of antitumor or protumor anesthetics (figure 1A, online supplemental table S1). These were then weighted through an RF training procedure (figure 1B, online supplemental table S2). Finally, anesthetic agents were submitted to hierarchical clustering based on their weighted molecular descriptors (figure 1C). Among the anesthetics for which no antitumor or protumor had been reported, DEX stood out in thus far that it clustered with the group of agents endowed with anticancer activity and that it is regularly used in the clinic.

To determine the potential antineoplastic activity of DEX, we first treated human osteosarcoma U2OS cells with different DEX concentrations and measured their proliferation and death at different time points (8, 12 or 24 hours). U2OS cells stopped proliferating and started dying at a concentration of 700–800 μ M DEX (figure 2A–C). Similar cytotoxic effects were observed for murine colorectal carcinoma CT26 cells, human colorectal adenocarcinoma HT29 cells, and murine fibrosarcoma MCA205 cells (online supplemental figure S1). DEX induced tumor cell death without an apoptotic intermediate step in which cells lose their mitochondrial transmembrane potential measured by means of DiOC before they become permeable to the vital dye DAPI (figure 2D). Neither z-VAD-fmk nor necrostatin-1, which are inhibitors of apoptosis and necrosis respectively, did inhibit the cytotoxic effects of DEX (figure 2E). Next, we investigated whether DEX would elicit specific cell stress. At sublethal doses, DEX activated specific signs of the unfolded protein response in the endoplasmic reticulum (ER) (figure 2F,G, online supplemental figure S2). Thus, DEX triggered the phosphorylation of eIF2 α detectable by immunofluorescence microscopy. In addition, DEX caused the nuclear translocation of ATF4 and ATF6 that could be measured in specific U2OS cell lines equipped with biosensor proteins, namely, ATF4 or ATF6 fused to GFP. However, DEX was unable to stimulate another sign of ER stress leading to the splicing of transcription factor X-box binding protein 1 (XBP1) messenger RNA that can be measured in a biosensor cell line expressing an XBP1-Venus fusion protein only after such a splicing event (figure 2F,G, online supplemental figure S2). In addition, DEX activated the formation of autophagic puncta in the cytoplasm of U2OS cells expressing microtubule-associated proteins 1A/1B LC3B fused to GFP. In the presence of bafilomycin A1, which inhibits the fusion of autophagosomes with lysosomes, DEX still induced GFP-LC3B puncta (as compared with the bafilomycin A1-only control) supporting the interpretation that DEX promotes autophagic flux (figure 2H,I). Similarly, DEX stimulated the autophagy-associated production of phosphatidylinositol 3-phosphate (PIP3), which

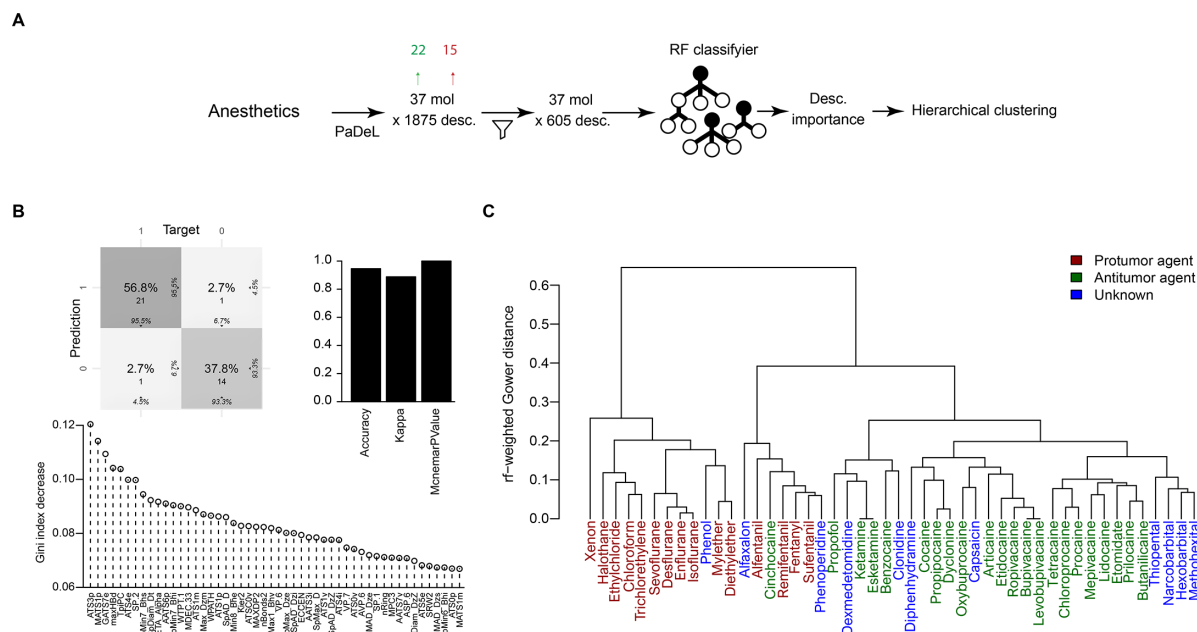


Figure 1 Trained Quantitative Structure-Activity Relationship (QSAR) model predicts dexmedetomidine as an antitumor agent A–C. (A) The main steps for the QSAR model establishment are represented as a flowchart. Molecular descriptors (desc) were computed using PaDEL software for a set of 37 molecules (mol), labeled according to their ability to act as antitumor or protumor agents ($n=22$ and $n=15$, respectively). The obtained data set was thereafter used for training a binary random forest (RF) classifier. Feature importance was extracted after the training process. (B) Classifier performance was evaluated by establishing a confusion matrix (upper left panel), from which different metrics were derived (upper right panel). Descriptors were ranked according to importance, represented by a decrease in Gini index (lower panel). (C) Molecules from the training set, plus 11 unknown agents, were used for hierarchical clustering using molecular descriptors weighted according to importance. Results are displayed in a clustering tree. Names in red and green correspond to protumor and antitumor compounds, respectively, used in the training set. Molecules with unknown or ambiguous effects on tumors are plotted in blue.

can be detected by means of a fusion protein containing RFP and the FYVE zinc domain. This fusion protein binds to PIP3-decorated vesicles, hence forming cytoplasmic puncta, which are induced by DEX (figure 2J,K).

In summary, DEX can trigger premortem stress, such as the unfolded protein response and autophagy, as well as the death of cancer cells.

DEX promotes immune anticancer effects *in vitro*.

Next, we studied whether DEX can stimulate immunogenic cell death (ICD), which occurs in the context of ER stress and autophagy. Similar to the established ICD inducer MTX,⁴¹ DEX elicited several hallmarks of ICD. Thus, immunofluorescence experiments indicated that DEX induced the translocation of CALR from the ER to the plasma membrane (figure 3A, online supplemental figure S3), in line with the fact that this event occurs downstream of the phosphorylation of eIF2 α and is inhibited by the IRE1 α /XBP1 pathway.³³ DEX also stimulated the extracellular release of HMGB1 protein measured by ELISA. Finally, DEX triggered the release of ATP from cells, as indicated by reduced intracellular ATP-dependent quinacrine fluorescence and the presence of luciferase-detectable ATP in the supernatant^{36,42} (figure 3B–D). In the next step, we cultured mouse fibrosarcoma MCA205 cells labeled with CellTracker Orange (CMTMR) in the presence of bone marrow-derived CD11c⁺ dendritic cells (BMDCs). Phagocytosis of tumor antigens was then

assessed by flow cytometry. DEX-treated cancer cells were more efficiently engulfed by BMDCs than untreated control cells and cells treated with the bona fide ICD inducer oxaliplatin (figure 3E–H).

Altogether these results suggest that DEX elicits the biomarkers of ICD and facilitates the engulfment of cancer cells by DCs.

DEX promotes an alpha-2 adrenoceptor-dependent anticancer response

To further investigate the immune effects of DEX, we orthotopically implanted subcutaneous MCA205 fibrosarcomas in immunocompetent C57Bl/6J mice. When tumors became palpable, mice were treated with either a single injection of DEX or daily injections of DEX for 21 days *i.p.*, mimicking anesthesia or intensive care practices, respectively. Daily administration of DEX, at doses used in veterinary medicine to induce a sedative effect in mice,⁴³ significantly reduced tumor growth and improved animal survival (online supplemental figures S4 and S5A,B). We confirmed these results for MC38 colon adenocarcinomas. Daily injection of DEX slowed down colon tumor growth and increased overall survival in a dose-dependent manner. The highest DEX dose (500 μ g/kg/day) reduced the size of tumors by up to 70% compared with untreated mice (figure 4A–E, online supplemental figure S5C). As an alternative to this high-dose systemic DEX administration, we designed experiments in which DEX was injected

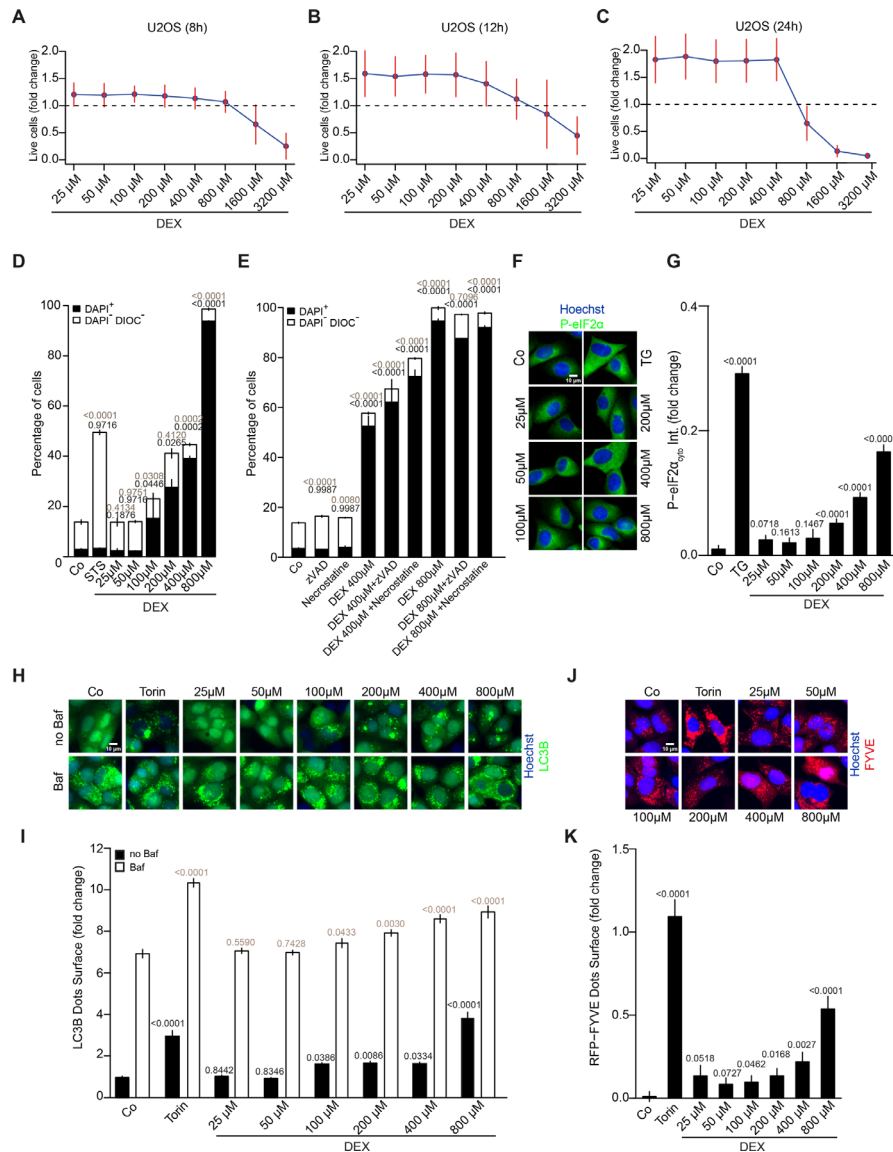


Figure 2 Premortem stress and cell death modalities promoted by dexmedetomidine A–K. (A–C) Human osteosarcoma U2OS wild-type (wt) cells were exposed to dexmedetomidine (DEX, 25 μ M, 50 μ M, 100 μ M, 200 μ M, 400 μ M, 800 μ M, 1,600 μ M or 3,200 μ M) for 8, 12 or 24 hours. Tumor cell death was assessed with the propidium iodide intensity. Number of live cells at each concentration was normalized to the number of live cells at T0. The dashed line represents a cytostatic effect. A proliferation effect is observed above the dashed line, while a cytolytic effect is observed below the dashed line. (D) U2OSwt cells were exposed to DEX (25 μ M, 50 μ M, 100 μ M, 200 μ M, 400 μ M or 800 μ M) or staurosporine (STS, 1 μ M) for 24 hours. Cell death was assessed by staining with DIOC and DAPI and data were acquired by flow cytometry. The data shown are presented as percentages of DIOC negative and DAPI negative (DIOC⁻ DAPI⁻) or DAPI positive cells alone (DAPI⁺). (E) U2OSwt cells were exposed to necrostatin-1 (10 μ M), z-VAD-fmk (zVAD, 50 μ M), dexmedetomidine (DEX, 400 μ M or 800 μ M), DEX+necrostatin-1 or DEX+zVAD for 24 hours. Cell death was assessed by the staining of DIOC and DAPI acquired by flow cytometry. The data shown are presented as percentages of DIOC⁻ DAPI⁻ or DAPI⁺ cells. Gray p value=DAPI⁻ DIOC⁻ comparison; Black p value=DAPI⁺ comparison. (F–G) U2OSwt cells were exposed to DEX (25 μ M, 50 μ M, 100 μ M, 200 μ M, 400 μ M or 800 μ M) or thapsigargin (TG, 10 μ M) for 6 hours. Phosphorylation of eIF2 α intensity was assessed by immunostaining. Representative images (F, scale bar 10 μ m). Bar plots (G). (H–I) U2OS GFP-LC3 cells were exposed to DEX (25 μ M, 50 μ M, 100 μ M, 200 μ M, 400 μ M or 800 μ M) or Torin (300 nM) with or without bafilomycin (Baf, 100 nM) for 8 hours. Autophagy was assessed by measuring the surface area occupied by GFP-LC3 dots. Representative images (H, scale bar 10 μ m). Bar plots (I). Black p values indicate treatment compared with untreated condition and gray p values indicate comparisons to bafilomycin. (J–K) U2OS XBP1s-venus-DBD cells were exposed to DEX (25 μ M, 50 μ M, 100 μ M, 200 μ M, 400 μ M or 800 μ M) or Torin (300 nM) for 12 hours. Autophagy was assessed by quantifying the dot surface. Representative images (J, scale bar 10 μ m). Bar plots (K). Information: (A, B, C, G, I, and K) data are presented as the mean \pm SEM of three individual experiments. Data were normalized to untreated control. (D and E) Data are presented as the mean \pm SD of one representative experiment among three. (D, E, and I) A pairwise test for multiple comparisons with a correction of Benjamini-Hochberg was applied. (G and K) The Student's t-test was applied. DAPI, 4,6-diamidino-2-phenylindole; DIOC, 3,3'-dihexyloxycarbocyanine iodide; eIF2 α , eukaryotic initiation factor 2 alpha; GFP, green fluorescent protein; RFP, red fluorescent protein.

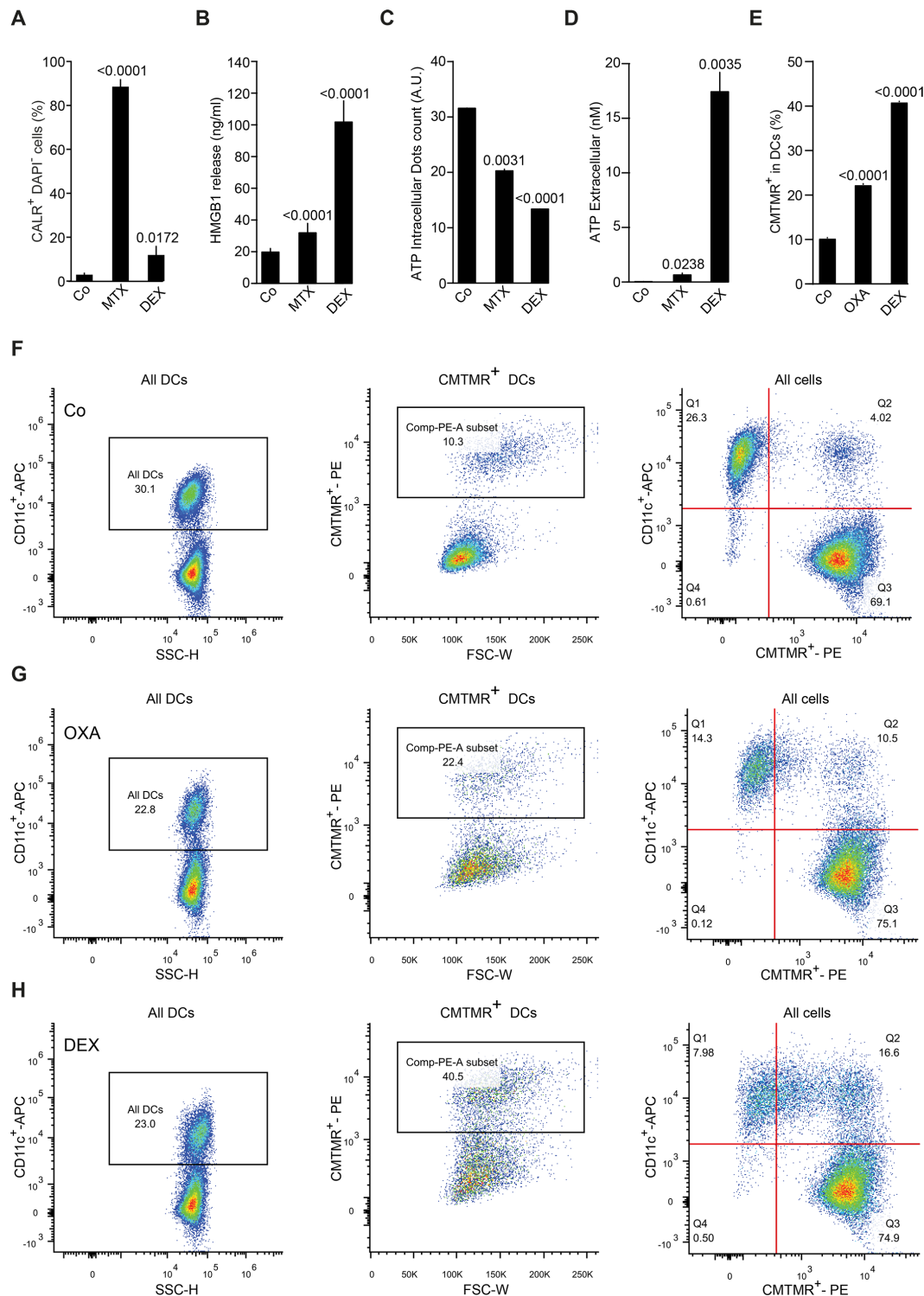


Figure 3 Dexmedetomidine induces immunogenic cell death and stimulates phagocytosis A–H. (A, C, D) U2OS human osteosarcoma wild-type (wt) or (B) MCA205wt murine fibrosarcoma were exposed to PBS (Co), mitoxantrone (MTX, 4 μ M) or dexmedetomidine (DEX, 600 μ M) for 8 hours (A) or 24 hours (B–D). (A) Calreticulin (CALR) exposure at the plasma membrane was measured by immunostaining acquired by flow cytometry. Data are presented as the percentage of CALR positive, DAPI negative (CALR⁺ DAPI⁻) cells. (B) HMGB1 release was assessed by ELISA. (C) Intracellular ATP decrease was measured by fluorescence microscopy. (D) Bioluminescence was used to measure the extracellular ATP release. (E–H) MCA205wt cells labeled with CellTracker Orange (CMTMR⁺) were exposed to oxaliplatin (Oxa, 300 μ M) or DEX (600 μ M) for 24 hours. The day after, tumor cells were co-cultured with bone marrow-derived dendritic cells (BMDCs) for 4 hours, and then stained with an antibody against CD11c (CD11c⁺-APC). The quantification of CMTMR⁺ and CD11c⁺ was obtained by flow cytometry. Information: data are presented as one representative experiment among two (or three for C) and expressed as mean \pm SD. Statistics were calculated using a Student's t-test. DAPI, 4,6-diamidino-2-phenylindole; HMGB1, high-mobility group box 1; PBS, phosphate-buffered saline.

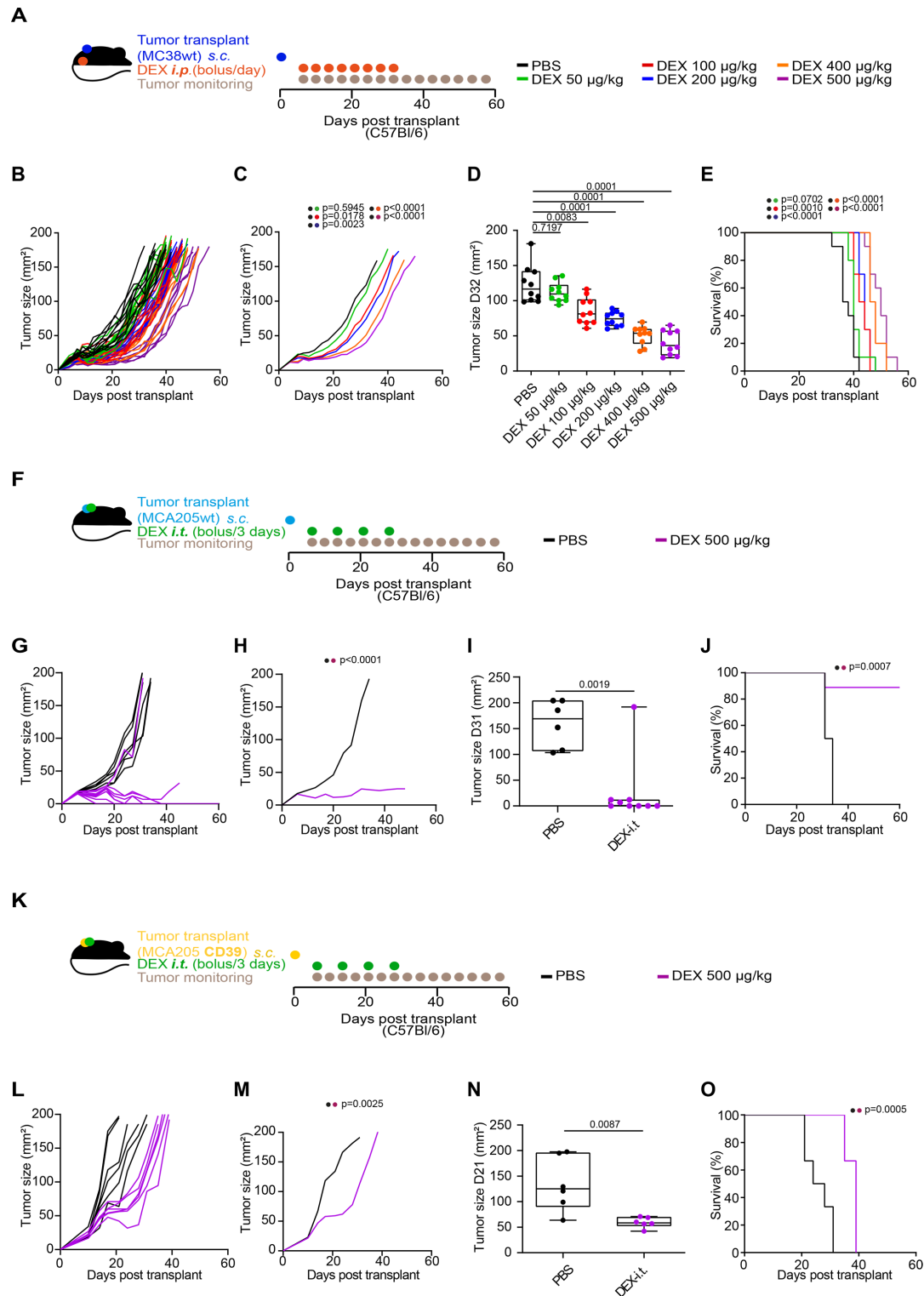


Figure 4 Dexmedetomidine induces an antitumor effect in vivo in a dose-dependent manner A–O. (A–E) 1×10^6 MC38 mouse colon adenocarcinoma wild-type (wt) cells were inoculated subcutaneously (s.c.) into the flank of C57Bl/6J mice (10 mice per group). When tumors became detectable, PBS (negative control) or dexmedetomidine (DEX, 50 µg/kg, 100 µg/kg, 200 µg/kg, 400 µg/kg or 500 µg/kg) was injected intraperitoneally (*i.p.*) every day for 21 days. (F–J) 1×10^5 MCA205wt mouse fibrosarcoma cells were inoculated s.c. into the flank of C57Bl/6J mice (6 mice for PBS group and 9 mice for DEX group). As soon as tumors became detectable, PBS (negative control) or DEX (500 µg/kg) was injected intratumorally (*i.t.*) every 3 days for 21 days. (K–O) 1×10^5 MCA205 cells expressing ectoATPase CD39 were inoculated s.c. into the flank of C57Bl/6J mice (6 mice per group). As soon as tumors became detectable, PBS (negative control) or DEX (500 µg/kg) was injected *i.t.* every 3 days for 21 days. Information: tumor size was compared using a type II ANOVA test and a pairwise Wilcoxon test with a Holm correction. Significant differences between overall survival were calculated by means of the log-rank test. ANOVA, analysis of variance; PBS, phosphate-buffered saline.

i.t., which is a route of administration of antineoplastic treatments that has been adopted in clinical practice.^{44–46} After *i.t.* injection of DEX into fibrosarcomas, 78% of mice were cured (figure 4F–J). Of note, this effect was mitigated when fibrosarcoma cells were equipped with a transgene-encoded ectoATPase degrading extracellular ATP (figure 4K–O).

DEX is a pan-ADRA2 agonist.³² Several mouse cancer cell lines such as breast cancers 4T1 and E0771, melanoma B16F10, colon adenocarcinoma CT26, fibrosarcoma MCA205 and lung cancer TC-1, express ADRA2 detectable by immunoblotting (online supplemental figure S6). We therefore investigated whether DEX acts on-target. For this, we determined the possible inhibitory effects of the pan-ADRA2 antagonist YOH on premortem stress responses induced by DEX *in vitro*. At concentrations of 10 μ M or 30 μ M, YOH decreased the phosphorylation of eIF2 α and autophagic flux induced by DEX (figure 5A–D). Then, we established murine fibrosarcomas MCA205 (figure 5E–I) or colon adenocarcinomas MC38 (online supplemental figure S7) in immunocompetent hosts and treated the mice with DEX alone or together with YOH. Importantly, YOH diminished the antitumor effects of DEX *in vivo*.

DEX modifies tumor infiltrates and potentiates immunotherapy effect *in vivo*

After injection of one single bolus, DEX decreased FoxP3⁺CD4⁺ Tregs in the tumor bed and increased the ratio of CD8⁺ cytotoxic T lymphocytes over Tregs in the tumor bed of MCA205 fibrosarcomas as well as in tumor-draining lymph nodes (figure 6, online supplemental figure S8). Moreover, DEX enhanced the co-expression of the checkpoint molecules lymphocyte activation gene 3 (LAG-3), PD-1, and T cell immunoglobulin and mucin 3 (TIM-3) on CD4⁺, CD8⁺ T cells and Tregs, indicating that it stimulates the accumulation of T cells with an exhausted phenotype (online supplemental figure S9). In line with this, the coadministration of anti-CD4⁺ and anti-CD8⁺ to mice bearing fibrosarcomas significantly decreased the anticancer effects of DEX (online supplemental figure S10). Surprisingly, one injection of DEX into mice bearing MC38 colon adenocarcinomas decreased (rather than increased) the CD8⁺/Tregs ratio in the tumor bed. In this tumor model, DEX reduced the co-expression of LAG-3, TIM-3 and PD-1 on CD4⁺ cells and Tregs (online supplemental figure S11A–F). The combination with YOH restored CD8⁺/Treg infiltration, but not the loss of checkpoint molecule expression (online supplemental figure S11G–I). Contrasting with a prior report on human tumors implanted in immunodeficient mice,⁴⁷ DEX did not affect biomarkers of tumor angiogenesis such as VEGF and CD31 in MCA205 fibrosarcomas (online supplemental figure S12).

Next, we evaluated whether DEX might be favorably combined with PD-1 blockade in four different models of solid tumors: MCA205 fibrosarcoma, MC38 colon adenocarcinoma, E0771 breast cancer, and RET melanoma

(figure 7). When tumors became palpable, mice received a daily injection of the optimal dose of DEX (500 μ g/kg *i.p.*) for 21 days alone or combined with three injections of anti-PD-1 antibody at days 6, 9 and 12 after the first injection of DEX. DEX alone significantly decreased tumor growth and improved overall survival in all four models. The combination with PD-1 blockade potentiated the effects of DEX and cured up to 50% of mice bearing fibrosarcomas. The responses to the DEX-anti-PD-1 combination treatment were variable, as shown by the increasing number of cured mice, in the following order: E0771 < MC38 < RET < MCA205 (figure 7). The combination of DEX and anti-PD-1 antibody was more efficient than DEX or anti-PD-1 alone in extending the survival of mice bearing MCA205 or RET but not E0771 and MC38 tumors (figure 7). We conclude that, depending on the tumor model, DEX induces a variably efficient anticancer immune response, and that DEX+PD-1 blockade may be favorably combined to control specific cancers.

Interestingly, in cured mice, rechallenge with identical cancer cells did not lead to the formation of tumors, suggesting the establishment of immune memory (online supplemental figure S13).

DISCUSSION

In this manuscript, we present an algorithm predicting the protumor or antitumor properties of anesthesia-relevant drugs. This algorithm was designed by a machine learning approach combining the molecular descriptors and the known protumor or antitumor effects of the drugs.²¹ To challenge this algorithm, we incorporated several molecules with unknown or ambiguous properties into our dataset. Most of them are historical anesthetics and no longer used clinically with the exception of DEX and clonidine. Clonidine has already been reported to mediate anticancer effects.⁴⁸ DEX is a sedative ADRA2 agonist clustered together with ketamine and propofol, as well as together with other agents including local anesthetics that are endowed with anticancer effects. Driven by this bioinformatic result, we decided to investigate the possible anticancer effects of DEX.

We found that, in cultured tumor cells, DEX activates two intertwined premortem stresses, namely (1) the integrated stress response (ISR) consisting in the phosphorylation of eIF2 α and (2) autophagy. In contrast to local anesthetics, which stimulate all three arms of the ER stress response (ie, (1) the ISR coupled to activation of ATF4, (2) the nuclear translocation of ATF6 and (3) the IRE1 α /XBP1 pathway),⁴⁹ DEX only stimulates two arms of the ER stress response, namely, (1) the ISR and (2) the activation of ATF6, but fails to induce the third arm consisting of the IRE1 α -mediated splicing of XBP1. The ISR is required to trigger autophagy⁵⁰ as well as the translocation of CALR from the ER to the cell surface,³³ and both these phenomena were induced by DEX.

Cancer cells treated with DEX also released ATP and HMGB1 *in vitro*. These DAMPs act as immunostimulatory

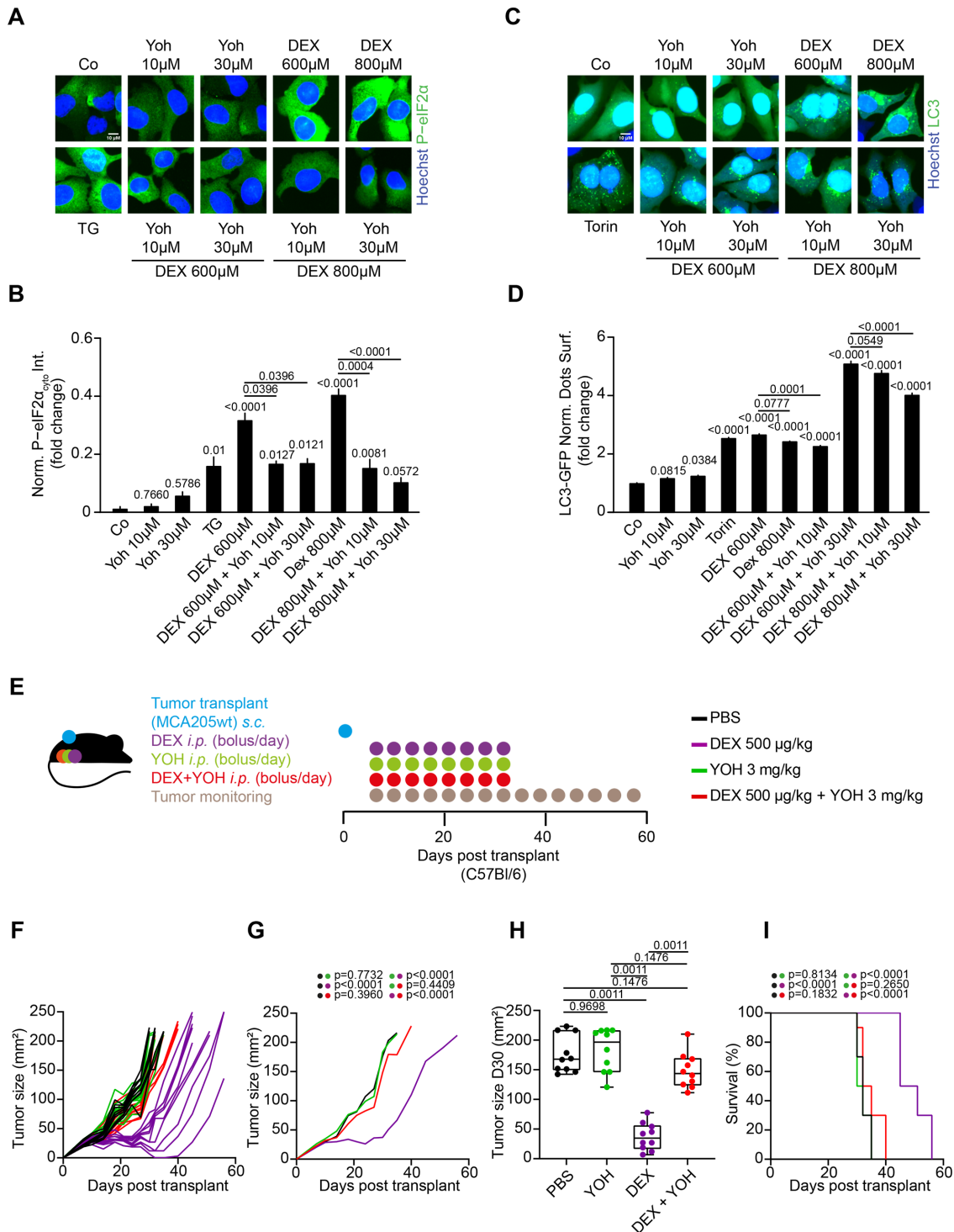


Figure 5 Antitumor effects of dexmedetomidine are mediated by alpha 2 adrenoceptors A–I. (A–B) Human osteosarcoma U2OS wild-type (wt) cells were exposed to DEX (600 μM or 800 μM) or thapsigargin (TG, 10 μM) or yohimbine (YOH 10 μM or 30 μM) or DEX+YOH for 6 hours. Phosphorylation of eIF2α intensity was assessed by immunostaining. Representative images (A, scale bar 10 μm). Bar plots (B). (C–D) U2OS GFP-LC3 cells were treated with DEX (600 μM or 800 μM) or Torin (300 nM) or YOH (10 μM or 30 μM) or DEX+YOH for 8 hours. Autophagy was quantified by measuring the dots' surface. Representative images (C, scale bar 10 μm). Bar plots (D). (E–I) 1 × 10⁵ murine fibrosarcoma MCA205wt cells were inoculated subcutaneously (s.c.) into the flank of C57Bl/6J mice. As soon as tumors became detectable, PBS (negative control), DEX (500 μg/kg), YOH (3 mg/kg) or DEX+YOH were injected every day for 21 days intraperitoneally (i.p.). Information: (B, D) data are shown as the mean ± SEM of two (B) or three (D) independent experiments. Data were normalized to untreated control. Significant differences were calculated using a pairwise test for multiple comparisons with a correction of Benjamini-Hochberg. (E–I) n = 10 mice for all groups. Tumor sizes were compared using a type II ANOVA test and a pairwise Wilcoxon test with a Holm correction. Significant differences between overall survival were calculated using the log-rank test. ANOVA, analysis of variance; DEX, dexmedetomidine; eIF2α, eukaryotic initiation factor 2 alpha; GFP, green fluorescent protein; PBS, phosphate-buffered saline.

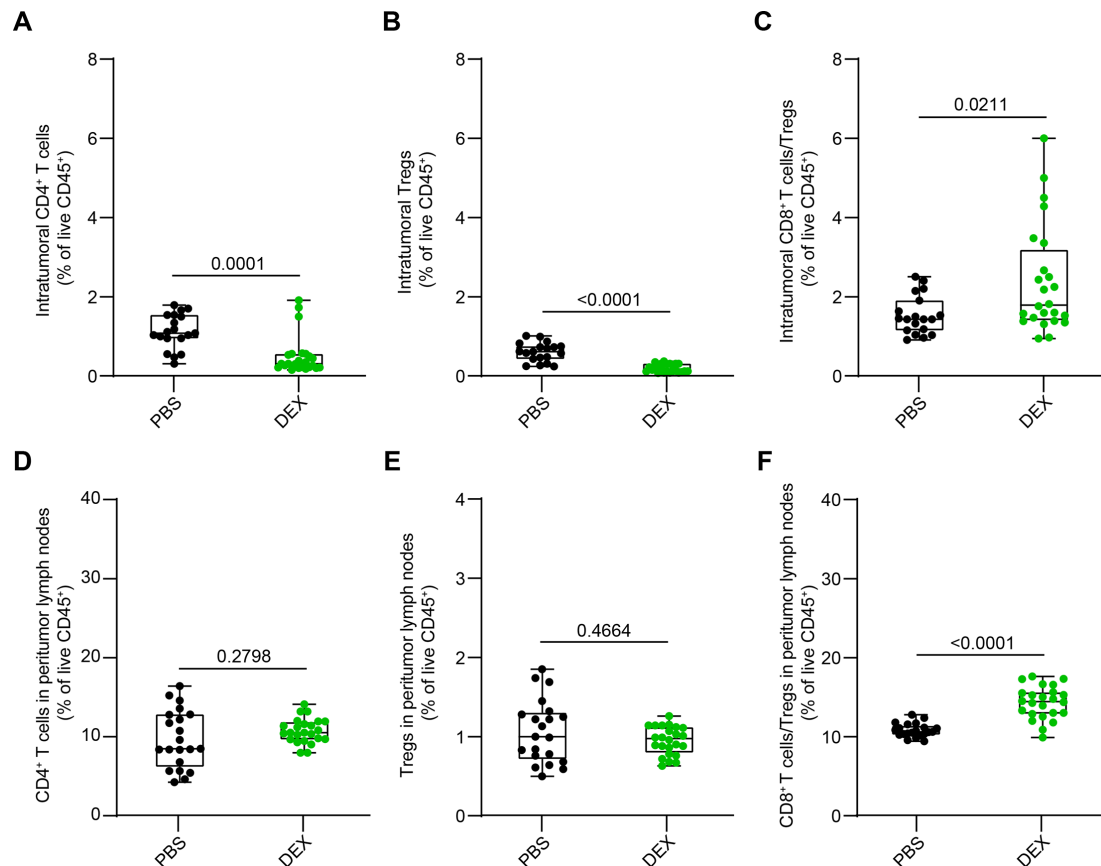


Figure 6 Dexmedetomidine influences tumor and peritumor lymph nodes-infiltrating lymphocyte subsets A–F. 1×10^5 murine fibrosarcoma MCA205 wild-type cells were inoculated subcutaneously (s.c.) into the flank of C57Bl/6J mice. As soon as tumors became detectable, one bolus of PBS or dexmedetomidine (DEX, 500 $\mu\text{g}/\text{kg}$ *i.p.*) was injected in mice (21 mice in PBS group and 24 mice in DEX group). Mice were sacrificed 9 days post-treatment and tumors were harvested. Lymphocyte T-cell subsets infiltrating the tumor bed and the peritumor lymph nodes were determined by immunostaining and flow cytometry (A–F). Information: p values were calculated by means of the Wilcoxon-Mann-Whitney test. Two aberrant values were removed from the PBS group (A–C). PBS, phosphate-buffered saline; Tregs, T regulatory cells.

agents that recruit and activate DCs.^{51–52} In line with this, we observed that DEX-treated cancer cells are efficiently engulfed by DCs. Of note, local anesthetics fail to stimulate CALR exposure, likely because they elicit the IRE1a/XBP1 pathway,²¹ which inhibits CALR exposure,⁵³ a fact that may explain why DEX has comparatively stronger anticancer effects than local anesthetics. In addition, the expression of an ectoATPase that degrades extracellular ATP in the vicinity of cancer cells^{33–36} inhibited the DEX-mediated antitumor response *in vivo*.

In various models of solid tumors established in immunocompetent mice, DEX decreased tumor growth and increased overall survival in a dose-dependent manner. However, a single bolus of DEX was sufficient to increase the ratio of CD8⁺ T cells over Tregs in the tumor bed, as well as in draining lymph nodes. Prior reports suggest that chemotherapeutics or targeted agents that induce ICD can sensitize tumors to subsequent immunotherapy with PD-1 blocking antibodies.^{54–56} Indeed, in at least two mouse cancer models (MCA205 fibrosarcoma and RET melanoma), the combination of DEX with anti-PD-1 monoclonal antibody (mAb) was more efficient than each of the therapeutic agents alone. Of note, DEX enhanced

the expression of exhaustion markers (LAG-3, TIM-3 and PD-1) on several tumor-infiltrating T cell subpopulations present in MCA205 fibrosarcomas. This goes in line with the observed combination effects of DEX and anti-PD-1 mAb. It will be interesting to investigate other combination effects (such as DEX+anti-LAG-3 or DEX+anti-TIM-3 mAbs) as well as higher-order combinations targeting several immune checkpoint molecules at once. It is noteworthy that DEX, used as a standalone agent after *i.p.* injection, is not sufficient to induce a long-term anti-cancer effect *in vivo*, as suggested by the recurrence of tumor growth on cessation of injections. However, intratumoral injection of high doses of DEX appears to be a promising route of administration, curing up to 78% of mice. Moreover, this cytolytic and direct effect, which can be attenuated by ADRA inhibitors,^{57–60} appears to be independent of the DEX-induced immune response, as it was conserved in nude mice, which lack T lymphocytes, as well as in mice bearing MC38 tumors without favorable alterations in the T-cell infiltrate.

Our work confirms that DEX triggers antitumor rather than protumor effects, and provides explanations for the contradictory properties of DEX that have previously been

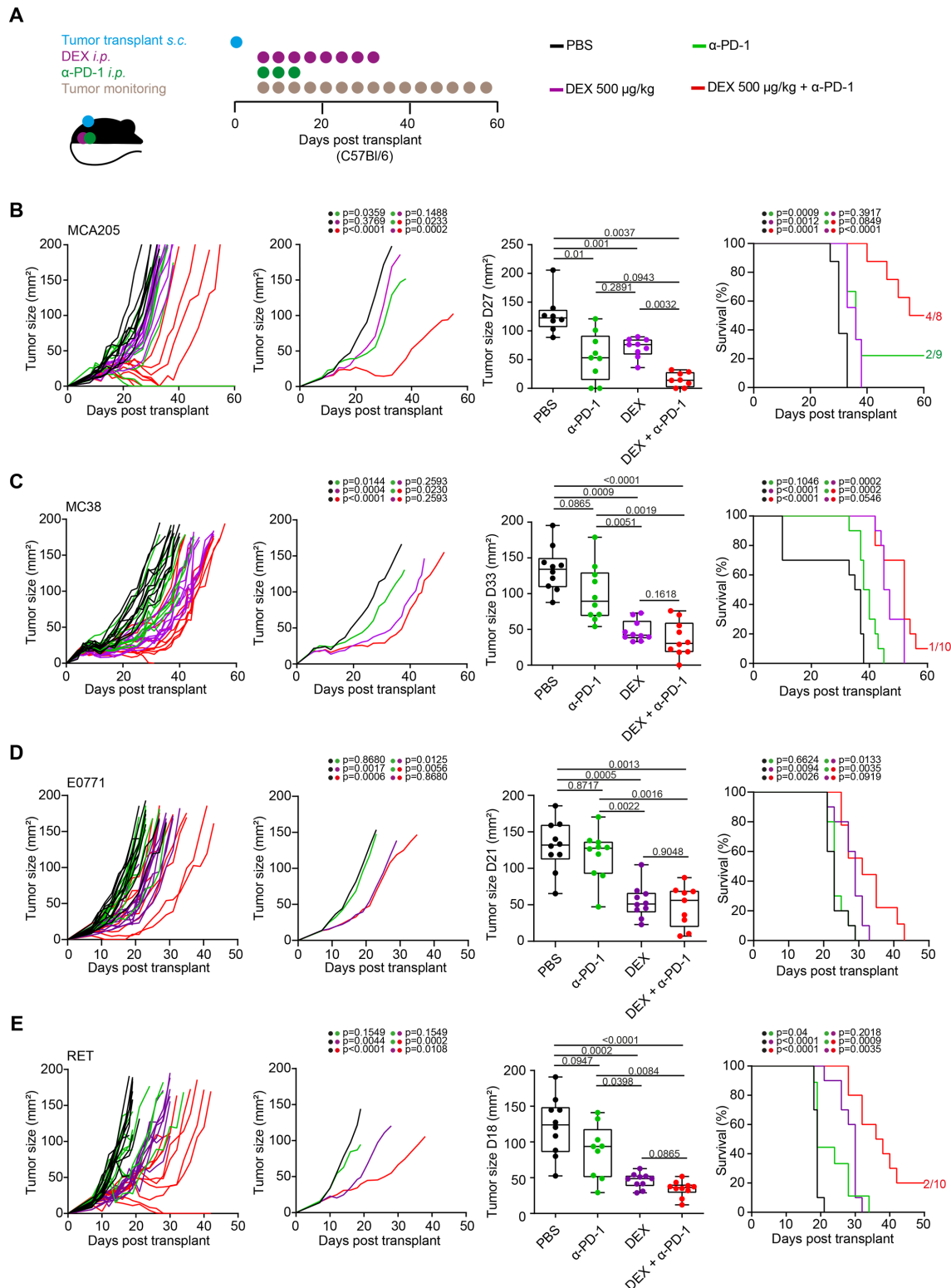


Figure 7 Dexmedetomidine elicits antitumor effects potentiated by anti-PD-1 in vivo A–E. (A) Experimental design. (B) 1×10^5 murine fibrosarcoma MCA205 wild-type (wt) cells, (C) 1×10^6 murine colon adenocarcinoma MC38wt cells, (D) 1×10^6 murine breast cancer E0771wt cells or (E) 5×10^5 murine RETwt melanoma cells were inoculated subcutaneously (s.c.) into the flank of C57Bl/6J mice. As soon as tumors became detectable, PBS (negative control) or dexmedetomidine (DEX, 500 μ g/kg) was injected intraperitoneally (*i.p.*) every day for 21 days. At days 6, 9 and 12 after the first injection of DEX, anti-PD-1 (200 μ g/mouse *i.p.*) or corresponding isotype was administered. Information: $n=10$ mice for all groups except: $n=9$ for anti-PD-1 (B, E), DEX (B), DEX+anti-PD-1 (D), $n=8$ for PBS and DEX+anti-PD-1 (B). Significant differences between tumor size were determined using a type II ANOVA test and a pairwise Wilcoxon test with a Holm correction. Significant differences between overall survival curves were calculated using the log-rank test. ANOVA, analysis of variance; PBS, phosphate-buffered saline; PD-1, programmed cell death protein 1.

described. Indeed, the action of DEX is dose-dependent, requiring a threshold concentration ($\geq 100 \mu\text{M}$ in vitro, best 1 mM in vitro, and $\geq 100 \mu\text{g/kg}$ in vivo, best $500 \mu\text{g/kg}$ in vivo) and daily injections for several weeks in vivo. One single injection of DEX failed to decrease tumor growth in vivo, in line with a prior study reporting that a single bolus of DEX ($25 \mu\text{g/kg}$) was unable to slow down the growth of E0771 breast tumors or MCA205 fibrosarcomas.⁶¹ One study reported that low-dose DEX ($10 \mu\text{g/kg}$) stimulated HIF-1 α /VEGF-dependent angiogenesis, while a higher dose ($25 \mu\text{g/kg}$) caused the opposite effect in human tumors.⁴⁷ Of note, angiogenesis markers such as VEGF and CD31 were not affected by DEX. Thus, our results are in line with a study demonstrating that clonidine, another ADRA2 agonist (with an affinity ~10 times lower than DEX) required a dosing of 5 mg/kg/day to inhibit tumor growth in mice.⁴⁸ Interestingly, our algorithm ranked clonidine close to DEX and among the anti-tumor anesthetics.

Our study has several limitations. First, the in vitro concentrations of DEX are very high compared with the plasma levels of DEX after *i.p.* injection, and similar concentrations of DEX seem difficult to achieve in the tumor microenvironment. Nevertheless, the tumor-eradicating effects of *i.t.* injected DEX, which should reach high local concentrations, plead in favor of local administration of DEX. Second, it remains an open question to which extent the anticancer effects of DEX are mediated on ADRA2 on cancer or immune cells and whether off-target effects (on other receptors than ADRA2) can be formally ruled out. Further experiments using knockout models in which ADRA2 is deleted in tumor cells or in the immune system would definitively address these important questions. Finally, it will be interesting to determine whether the association with anti-PD-1 antibody further potentiates the already quite efficient effects of the *i.t.* injection of DEX, and whether DEX injected into one single malignant lesion may induce effects that affect distant, non-injected metastases of the primary tumor as well. Such abscopal effects might be investigated in the absence and presence of immune checkpoint blockade.

Intensive care may favor tumor progression because antineoplastic treatments are discontinued during this critical period. In this context, continuous sedation with DEX might be useful to prevent tumor progression. Obviously, this hypothesis needs to be confirmed in prospective randomized controlled trials. Hitherto, very few trials have investigated oncological outcomes after DEX administration. Unfortunately, these trials were inconclusive due to their retrospective nature, confounding bias (DEX in all trial arms, short infusion of DEX), or lack of inclusions.^{62 63} Other ongoing trials are evaluating the impact of continuous infusion of DEX on overall and recurrence-free survival after surgical removal of breast, colorectal or non-specified solid tumors (NCT05742438, NCT04106999, NCT03012971, NCT06030804, NCT03109990, NCT03370588).

In conclusion, our work validated an algorithm predicting the antitumor or protumor properties of anesthetics. This algorithm correctly predicted that DEX is a potent anticancer agent, as we confirmed by preclinical experimentation. Of note DEX efficiently sensitized tumors to PD-1 blockade. Future trials must explore the utility of DEX-based sedation during intensive care of oncological patients.

X Guido Kroemer @None

Acknowledgements We thank the animal facilities, the AMMICA-PETRA platform, the cytometry platform of Gustave Roussy, the Université Paris-Saclay, and ESAIC-RG-EP.

Contributors LZ, PL, and LB realized most experiments and analyses. AS designed the machine learning approach. JP, AC and JL participated in the tumor immune infiltrate experiments. KCLP performed ATP experiments. OK conceived figure design. GK and LB designed the project and wrote the manuscript. All authors reviewed the manuscript. All authors approved the final version of the manuscript. All authors agreed to be accountable for their work. GK and LB are the guarantors of the manuscript.

Funding OK has the support of Institut National du Cancer (INCa) and the Association pour la recherche sur le cancer (ARC). GK has the support of the Agence National de la Recherche (ANR) – Projets blancs; AMMICA US23/CNRS UMS3655; ARC; Cancéropôle Ile-de-France; Fondation pour la Recherche Médicale (FRM); the Carrefour foundation; Crimson (No. 101016923); Elior; Equipex Onco-Pheno-Screen (ANR 21-ESRE-0028); European Joint Programme on Rare Diseases (EJPRD); European Research Council Advanced Investigator Award (ERC-2021-ADG, ICD-Cancer, Grant No. 101052444), European Union Horizon 2020; INCa; Institut Universitaire de France; LabEx Immuno-Oncology (ANR-18-IDEX-0001); the Ligue contre le Cancer (équipe labellisée); Projects Oncobiome, Prevalung (grant No. 101095604); a Cancer Research ASPIRE Award from the Mark Foundation; the RHU Immunolife; the Seerave Foundation; the SIRIC Stratified Oncology Cell DNA Repair and Tumor Immune Elimination (SOCRATE); the SIRIC Cancer Research and Personalized Medicine (CARPEM). LB is supported by the Société Française d'Anesthésie Réanimation (SFAR), La Ligue contre le Cancer, The Monahan Foundation, and The Philippe Foundation.

Competing interests OK is one of the co-founders of Samsara Therapeutics. GK has some contracts with Daiichi Sankyo, Vascage, Eleor, Tolllys, Kaleido, Sutro, Lytix Pharma, Sanofi, PharmaMar, Samsara Therapeutics, and Osasuna Therapeutics. GK belongs to the Board of the Bristol Myers Squibb Foundation in France. GK is one of the co-founders of EverImmune, Therafast Bio, Samsara Therapeutics, and Osasuna Therapeutics. GK is in the scientific boards of Rejuveron Life Sciences, Hevolution, Longevity Vision Funds, and Institut Servier. GK has some patents covering therapeutics dealing with cancer, aging, metabolic diseases, and cystic fibrosis. The brother of GK, Romano Kroemer, worked for Sanofi company and is now employee of Boehringer-Ingelheim. The wife of GK, Laurence Zitvogel, has some scientific contracts with Daiichi Sankyo, Glaxo Smith Kline, Incyte, Innovate Pharma, Kaleido, Lytix, Merus, Pilege, Roche, Transgene, 9 m, and Tusk, and was in the Board of Transgene, is one of the co-founders of EverImmune, and holds patents dealing with microbiota and cancer. The funders had no role in the design, writing or publication of the manuscript. JP has some patents dealing with cancer vaccination (Turnstone Biologics).

Patient consent for publication Not applicable.

Ethics approval In vivo experiments were conducted in the respect of the EU Directive 63/2010. All protocols were approved by the Ethical committee of Gustave Roussy (CEEA IRCIV/IGR no.26) and were registered at the French Ministry of Research with the following references: 202211281443211v3, 2023100307224938v3.

Provenance and peer review Not commissioned; externally peer reviewed.

Data availability statement Data are available upon reasonable request. Data are available from the corresponding author on reasonable request.

Supplemental material This content has been supplied by the author(s). It has not been vetted by BMJ Publishing Group Limited (BMJ) and may not have been peer-reviewed. Any opinions or recommendations discussed are solely those of the author(s) and are not endorsed by BMJ. BMJ disclaims all liability and responsibility arising from any reliance placed on the content. Where the content

includes any translated material, BMJ does not warrant the accuracy and reliability of the translations (including but not limited to local regulations, clinical guidelines, terminology, drug names and drug dosages), and is not responsible for any error and/or omissions arising from translation and adaptation or otherwise.

Open access This is an open access article distributed in accordance with the Creative Commons Attribution Non Commercial (CC BY-NC 4.0) license, which permits others to distribute, remix, adapt, build upon this work non-commercially, and license their derivative works on different terms, provided the original work is properly cited, appropriate credit is given, any changes made indicated, and the use is non-commercial. See <http://creativecommons.org/licenses/by-nc/4.0/>.

ORCID iDs

Jonathan Pol <http://orcid.org/0000-0002-8355-7562>

Oliver Kepp <http://orcid.org/0000-0002-6081-9558>

Guido Kroemer <http://orcid.org/0000-0002-9334-4405>

Lucillia Bezu <http://orcid.org/0000-0002-3569-6066>

REFERENCES

- Brogi E, Forfori F. Anesthesia and cancer recurrence: an overview. *J Anesth Analg Crit Care* 2022;2:33.
- Carnet Le Provost K, Kepp O, Kroemer G, et al. Trial watch: local anesthetics in cancer therapy. *Oncoimmunology* 2024;13:2308940.
- Deegan CA, Murray D, Doran P, et al. Anesthetic technique and the cytokine and matrix metalloproteinase response to primary breast cancer surgery. *Reg Anesth Pain Med* 2010;35:490–5.
- Piegeler T, Schlöpfer M, Dull RO, et al. Clinically relevant concentrations of lidocaine and ropivacaine inhibit TNF α -induced invasion of lung adenocarcinoma cells in vitro by blocking the activation of Akt and focal adhesion kinase. *Br J Anaesth* 2015;115:784–91.
- Chen J, Jiao Z, Wang A, et al. Lidocaine inhibits melanoma cell proliferation by regulating ERK phosphorylation. *J of Cellular Biochemistry* 2019;120:6402–8.
- Zhang L, Hu R, Cheng Y, et al. Lidocaine inhibits the proliferation of lung cancer by regulating the expression of GOLTA. *Cell Prolif* 2017;50:e12364.
- Le Gac G, Angenard G, Clément B, et al. Local Anesthetics Inhibit the Growth of Human Hepatocellular Carcinoma Cells. *Anesth Analg* 2017;125:1600–9.
- Castelli V, Piroli A, Marinangeli F, et al. Local anesthetics counteract cell proliferation and migration of human triple-negative breast cancer and melanoma cells. *J Cell Physiol* 2020;235:3474–84.
- Tada M, Imazeki F, Fukai K, et al. Procaine inhibits the proliferation and DNA methylation in human hepatoma cells. *Hepatol Int* 2007;1:355–64.
- Qin A, Liu Q, Wang J. Ropivacaine inhibits proliferation, invasion, migration and promotes apoptosis of papillary thyroid cancer cells via regulating ITGA2 expression. *Drug Dev Res* 2020;81:700–7.
- Kwakye AK, Kampo S, Lv J, et al. Levobupivacaine inhibits proliferation and promotes apoptosis of breast cancer cells by suppressing the PI3K/Akt/mTOR signalling pathway. *BMC Res Notes* 2020;13:386.
- Huang Y, Lei L, Liu Y. Propofol Improves Sensitivity of Lung Cancer Cells to Cisplatin and Its Mechanism. *Med Sci Monit* 2020;26:e919786.
- Zhang Y-F, Li C-S, Zhou Y, et al. Effects of propofol on colon cancer metastasis through STAT3/HOTAIR axis by activating WIF-1 and suppressing Wnt pathway. *Cancer Med* 2020;9:1842–54.
- Wang Z, Cao B, Ji P, et al. Propofol inhibits tumor angiogenesis through targeting VEGF/VEGFR and mTOR/eIF4E signaling. *Biochem Biophys Res Commun* 2021;555:13–8.
- Cao Y, Fan L, Li L, et al. Propofol suppresses cell proliferation in gastric cancer cells through NRF2-mediated polyol pathway. *Clin Exp Pharmacol Physiol* 2022;49:264–74.
- Zhang N, Xing X, Gu F, et al. Ropivacaine Inhibits the Growth, Migration and Invasion of Gastric Cancer Through Attenuation of WEE1 and PI3K/AKT Signaling via miR-520a-3p. *Onco Targets Ther* 2020;13:5309–21.
- Li C, Gao S, Li X, et al. Procaine Inhibits the Proliferation and Migration of Colon Cancer Cells Through Inactivation of the ERK/MAPK/FAK Pathways by Regulation of RhoA. *Oncol Res* 2018;26:209–17.
- Wang H-L, Yan H-D, Liu Y-Y, et al. Intraoperative intravenous lidocaine exerts a protective effect on cell-mediated immunity in patients undergoing radical hysterectomy. *Mol Med Rep* 2015;12:7039–44.
- Zhou D, Gu F-M, Gao Q, et al. Effects of anesthetic methods on preserving anti-tumor T-helper polarization following hepatectomy. *World J Gastroenterol* 2012;18:3089–98.
- Wu Chuang A, Kepp O, Kroemer G, et al. Direct Cytotoxic and Indirect, Immune-Mediated Effects of Local Anesthetics Against Cancer. *Front Oncol* 2021;11:821785.
- Bezu L, Wu Chuang A, Sauvat A, et al. Local anesthetics elicit immune-dependent anticancer effects. *J Immunother Cancer* 2022;10:e004151.
- Zhang W, Xue F, Xie S, et al. Isoflurane promotes proliferation of squamous cervical cancer cells through mTOR-histone deacetylase 6 pathway. *Mol Cell Biochem* 2021;476:45–55.
- Lu N, Piao M-H, Feng C-S, et al. Isoflurane promotes epithelial-to-mesenchymal transition and metastasis of bladder cancer cells through HIF-1 α - β -catenin/Notch1 pathways. *Life Sci* 2020;258:118154.
- Liu Z, Cheng S, Fu G, et al. Postoperative administration of ketorolac averts morphine-induced angiogenesis and metastasis in triple-negative breast cancer. *Life Sci (1962)* 2020;251:117604.
- Levi L, Hikri E, Popovtzer A, et al. Effect of Opioid Receptor Activation and Blockage on the Progression and Response to Treatment of Head and Neck Squamous Cell Carcinoma. *J Clin Med* 2023;12:1277.
- Di Franco C, Evangelista F, Briganti A. Multiple uses of dexmedetomidine in small animals: a mini review. *Front Vet Sci* 2023;10:1135124.
- Afonso J, Reis F. Dexmedetomidine: current role in anesthesia and intensive care. *Rev Bras Anesthesiol* 2012;62:118–33.
- Weatherall M, Aantaa R, Conti G, et al. A multinational, drug utilization study to investigate the use of dexmedetomidine (Dexdor®) in clinical practice in the EU. *Br J Clin Pharmacol* 2017;83:2066–76.
- Correa-Sales C, Rabin BC, Maze M. A hypnotic response to dexmedetomidine, an alpha 2 agonist, is mediated in the locus coeruleus in rats. *Anesthesiology* 1992;76:948–52.
- Xia M, Ji N-N, Duan M-L, et al. Dexmedetomidine regulate the malignancy of breast cancer cells by activating α 2-adrenoceptor/ERK signaling pathway. *Eur Rev Med Pharmacol Sci* 2016;20:3500–6.
- Wang C, Datto T, Zhao H, et al. Midazolam and Dexmedetomidine Affect Neuroglioma and Lung Carcinoma Cell Biology In Vitro and In Vivo. *Anesthesiology* 2018;129:1000–14.
- Carnet Le Provost K, Kepp O, Kroemer G, et al. Trial watch: dexmedetomidine in cancer therapy. *Oncoimmunology* 2024;13:2327143.
- Bezu L, Sauvat A, Humeau J, et al. eIF2 α phosphorylation is pathognomonic for immunogenic cell death. *Cell Death Differ* 2018;25:1375–93.
- Martins I, Kepp O, Schlemmer F, et al. Restoration of the immunogenicity of cisplatin-induced cancer cell death by endoplasmic reticulum stress. *Oncogene* 2011;30:1147–58.
- Senovilla L, Vitale I, Martins I, et al. An immunosurveillance mechanism controls cancer cell ploidy. *Science* 2012;337:1678–84.
- Michaud M, Martins I, Sukkurwala AQ, et al. Autophagy-dependent anticancer immune responses induced by chemotherapeutic agents in mice. *Science* 2011;334:1573–7.
- Yap CW. PaDEL-descriptor: an open source software to calculate molecular descriptors and fingerprints. *J Comput Chem* 2011;32:1466–74.
- Enot DP, Vacchelli E, Jacquelinot N, et al. TumGrowth: An open-access web tool for the statistical analysis of tumor growth curves. *Oncoimmunology* 2018;7:e1462431.
- Badwe RA, Parmar V, Nair N, et al. Effect of Peritumoral Infiltration of Local Anesthetic Before Surgery on Survival in Early Breast Cancer. *J Clin Oncol* 2023;41:3318–28.
- Carnet Le Provost K, Kepp O, Kroemer G, et al. Trial watch: beta-blockers in cancer therapy. *Oncoimmunology* 2023;12:2284486.
- Obeid M, Tesniere A, Ghiringhelli F, et al. Calreticulin exposure dictates the immunogenicity of cancer cell death. *Nat Med* 2007;13:54–61.
- Apetoh L, Ghiringhelli F, Tesniere A, et al. Toll-like receptor 4-dependent contribution of the immune system to anticancer chemotherapy and radiotherapy. *Nat Med* 2007;13:1050–9.
- Oh SS, Narver HL. Mouse and Rat Anesthesia and Analgesia. *Curr Protoc* 2024;4:e995.
- Tselikas L, de Baere T, Isoardo T, et al. Pickering emulsions with ethiodized oil and nanoparticles for slow release of intratumoral anti-CTLA4 immune checkpoint antibodies. *J Immunother Cancer* 2020;8:e000579.
- Champliat S, Tselikas L, Farhane S, et al. Intratumoral Immunotherapy: From Trial Design to Clinical Practice. *Clin Cancer Res* 2021;27:665–79.

- 46 Tselikas L, Dardenne A, de Baere T, *et al.* Feasibility, safety and efficacy of human intra-tumoral immuno-therapy. Gustave Roussy's initial experience with its first 100 patients. *Eur J Cancer* 2022;172:1–12.
- 47 Fang T, Lin L, Ye ZJ, *et al.* Dexmedetomidine Promotes Angiogenesis and Vasculogenic Mimicry in Human Hepatocellular Carcinoma through α_2 -AR/HIF-1 α /VEGFA Pathway. *Biomed Environ Sci* 2022;35:931–42.
- 48 Zhu J, Naulaerts S, Boudhan L, *et al.* Tumour immune rejection triggered by activation of α_2 -adrenergic receptors. *Nature New Biol* 2023;618:607–15.
- 49 Walter P, Ron D. The unfolded protein response: from stress pathway to homeostatic regulation. *Science* 2011;334:1081–6.
- 50 Høyer-Hansen M, Jäättelä M. Connecting endoplasmic reticulum stress to autophagy by unfolded protein response and calcium. *Cell Death Differ* 2007;14:1576–82.
- 51 Galluzzi L, Guilbaud E, Schmidt D, *et al.* Targeting immunogenic cell stress and death for cancer therapy. *Nat Rev Drug Discov* 2024;23:445–60.
- 52 Kroemer G, Galassi C, Zitvogel L, *et al.* Immunogenic cell stress and death. *Nat Immunol* 2022;23:487–500.
- 53 Pozzi C, Cuomo A, Spadoni I, *et al.* The EGFR-specific antibody cetuximab combined with chemotherapy triggers immunogenic cell death. *Nat Med* 2016;22:624–31.
- 54 Pan H, Liu P, Kroemer G, *et al.* Preconditioning with immunogenic cell death-inducing treatments for subsequent immunotherapy. *Int Rev Cell Mol Biol* 2024;382:279–94.
- 55 Kepp O, Kroemer G. Immunogenic Cell Stress and Death Sensitize Tumors to Immunotherapy. *Cells* 2023;12:2843.
- 56 Pan H, Liu P, Zhao L, *et al.* Immunogenic cell stress and death in the treatment of cancer. *Semin Cell Dev Biol* 2024;156:11–21.
- 57 Zhang W, Zhang L, Cai X-J, *et al.* Dexmedetomidine inhibits the growth and metastasis of esophageal cancer cells by down-regulation of lncRNA MALAT1. *Kaohsiung J Med Sci* 2022;38:585–93.
- 58 Jun JH, Shim J-K, Oh JE, *et al.* Effects of dexmedetomidine on A549 non-small cell lung cancer growth in a clinically relevant surgical xenograft model. *Sci Rep* 2023;13:12471.
- 59 Gao X, Wang XL. Dexmedetomidine promotes ferroptotic cell death in gastric cancer via hsa_circ_0008035/miR-302a/E2F7 axis. *Kaohsiung J Med Sci* 2023;39:390–403.
- 60 Shin S, Kim KJ, Hwang HJ, *et al.* Immunomodulatory Effects of Perioperative Dexmedetomidine in Ovarian Cancer: An *In Vitro* and Xenograft Mouse Model Study. *Front Oncol* 2021;11:722743.
- 61 Chen W, Qi Z, Fan P, *et al.* Dexmedetomidine provides type-specific tumour suppression without tumour-enhancing effects in syngeneic murine models. *Br J Anaesth* 2023;130:142–53.
- 62 Cata JP, Nguyen LT, Ifeanyi-Pillette IC, *et al.* An assessment of the survival impact of multimodal anesthesia/analgesia technique in adults undergoing cytoreductive surgery with hyperthermic intraperitoneal chemotherapy: a propensity score matched analysis. *Int J Hyperthermia* 2019;36:369–75.
- 63 Rangel FP, Auler JOC Jr, Carmona MJC, *et al.* Opioids and premature biochemical recurrence of prostate cancer: a randomised prospective clinical trial. *Br J Anaesth* 2021;126:931–9.